Efficient flavinylation of glycosomal fumarate reductase by its own ApbE domain in Trypanosoma brucei

Robin Schenk, Sabine Bachmaier, Frédéric Bringaud, Michael Boshart

The FEBS Journal

FEBS PRESS science publishing by scientists

Efficient flavinylation of glycosomal fumarate reductase by its own ApbE domain in *Trypanosoma brucei*

Robin Schenk[1], Sabine Bachmaier[1], Frédéric Bringaud[2] and Michael Boshart[1]

1 Biozentrum, Fakultät für Biologie, Genetik, Ludwig-Maximilians-Universität München (LMU), Martinsried, Germany
2 CNRS, Microbiologie Fondamentale et Pathogénicité (MFP), UMR 5234, Université de Bordeaux, France

Keywords
ApbE; flavin transferase; fluorescent tag; fumarate reductase; glycosome

Correspondence
M. Boshart, Biozentrum, Fakultät für Biologie, Genetik, Ludwig-Maximilians-Universität München (LMU), 82152, Planegg-Martinsried, Germany
Tel: +49 89 2180 74600
E-mail: boshart@lmu.de

(Received 30 December 2020, revised 8 February 2021, accepted 9 March 2021)

doi:10.1111/febs.15812

A subset of flavoproteins has a covalently attached flavin prosthetic group enzymatically attached via phosphoester bonding. In prokaryotes, this is catalysed by alternative pyrimidine biosynthesis E (ApbE) flavin transferases. ApbE-like domains are present in few eukaryotic taxa, for example the N-terminal domain of fumarate reductase (FRD) of *Trypanosoma*, a parasitic protist known as a tropical pathogen causing African sleeping sickness. We use the versatile reverse genetic tools available for *Trypanosoma* to investigate the flavinylation of glycosomal FRD (FRDg) *in vivo* in the physiological and organellar context. Using direct in-gel fluorescence detection of covalently attached flavin as proxy for activity, we show that the ApbE-like domain of FRDg has flavin transferase activity *in vivo*. The ApbE domain is preceded by a consensus flavinylation target motif at the extreme N terminus of FRDg, and serine 9 in this motif is essential as flavin acceptor. The preferred mode of flavinylation in the glycosome was addressed by stoichiometric expression and comparison of native and catalytically inactive ApbE domains. In addition to the *trans*-flavinylation activity, the ApbE domain catalyses the intramolecular *cis*-flavinylation with at least fivefold higher efficiency. We discuss how the higher efficiency due to unusual fusion of the ApbE domain to its substrate protein FRD may provide a selective advantage by faster FRD biogenesis during rapid metabolic adaptation of trypanosomes. The first 37 amino acids of FRDg, including the consensus motif, are sufficient as flavinylation target upon fusion to other proteins. We propose FRDg(1-37) as 4-kDa heat-stable, detergent-resistant fluorescent protein tag and suggest its use as a new tool to study glycosomal protein import.

Introduction

Flavoproteins are ubiquitous redox proteins associated with an eponymous flavin molecule, most commonly, flavin adenine dinucleotide (FAD) or its precursor, flavin mononucleotide (FMN). A defining feature shared by those cofactors is the isoalloxazine ring (Fig. 1), a tricyclic structure, which introduces a wide variety of chemical and physical properties, in particular when incorporated into the active centre of enzymes. Versatility of catalytic reactions is exemplified by numerous oxidases, reductases, dehydrogenases, electron

Abbreviations
ACO, aconitase; ApbE, alternative pyrimidine biosynthesis E; BSF, bloodstream form; ENO, enolase; FAD, flavin adenine dinucleotide; FbFP, flavin-based fluorescent protein; FMN, flavin mononucleotide; FRD, fumarate reductase; FRDg, glycosomal fumarate reductase; FRDm, mitochondrial fumarate reductase; FTM, flavinylation target motif; HSP60, heat-shock protein 60; IDHg, glycosomal isocitrate dehydrogenase; LOV, light–oxygen–voltage; PCF, procyclic form; PFR, paraflagellar rod; PPDK, pyruvate phosphate dikinase; SDH, succinate dehydrogenase; tet, tetracycline.

transferases, mediating both one- and two-electron transfer. Flavoproteins also include DNA damage repair proteins and photochemical signalling components [1–4]. Blue-light photoreceptors and bacterial luciferases [5,6] utilise the distinct fluorescent properties of flavins for their function [7]. They typically feature excitation/emission maxima of the oxidised form at around 450/520 nm, depending on environmental conditions and binding partners [8,9]. The optical properties do not only allow characterisation of specific flavoproteins and their state transitions [10,11], but also visualisation of flavin-rich cell populations or subcellular structures such as mitochondria [12,13].

Flavin cofactors are mostly tight binding and structurally shielded, presumably to prevent interaction with molecular oxygen and subsequent production of H_2O_2 [2,14]. Yet, noncovalent binding strongly prevails, with only ~ 10% of flavoproteins being covalently flavinylated [15]. This minority of enzymes has an increased redox potential allowing for thermodynamically demanding reactions and more efficient substrate turnover, as well as higher holoenzyme stability due to fixation of the cofactor [15,16]. Mechanistically, linkage of cysteine, tyrosine or histidine to the 8α-methyl group or the C6 atom of the isoalloxazine ring (Fig. 1) has been reported and suggested to occur autocatalytically [17]. Alternatively, in prokaryotes flavin transferases of the ApbE (alternative pyrimidine biosynthesis; also Ftp: flavin-trafficking protein) family (PFAM ID: PF02424) attach FMN covalently to threonine residues by phosphoester bond formation [18,19]. ApbE recognises the degenerated consensus sequence Dxx(s/t)gAT and targets threonine 7 in this motif as the FMN acceptor residue [20,21]. A well-described target of ApbE-mediated post-translational modification is Na^+-translocating NADH:quinone oxidoreductase, a component of the respiratory chain [18,22].

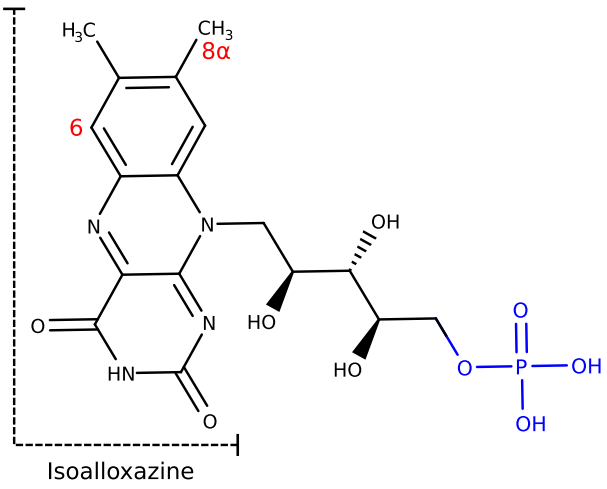

Fig. 1. Structure of oxidised FMN. The C6 atom and the 8α-methyl groups, which are subject to autocatalytic protein attachment, are labelled in red. The phosphate group esterified by ApbE with the acceptor threonine or serine is highlighted in blue. MarvinSketch 20.13.0 (https://chemaxon.com/products/marvin) was used for chemical drawing.

Fumarate reductases (FRDs), which catalyse the reduction of fumarate to succinate during anaerobic metabolism [23,24], predominantly occur as multisubunit membrane-bound complexes. In bacteria, the FRD periphery is exposed to the cytoplasm, in eukaryotes to the mitochondrial matrix, transferring electrons from quinol to the terminal electron acceptor fumarate. In some organisms, a second type of FRD is found that is soluble and monomeric, oxidises FADH2, FMNH2 or NADH in place of quinol [25] and contains a cytochrome domain instead of an iron sulphur cluster subunit [26]. Both classes of FRD further contain a prosthetic flavin group [23]. Evidence points to autocatalytic linkage of flavin to membrane-bound FRD in *E. coli* [27,28], while flavinylation of human succinate dehydrogenase (SDH) subunit A, which is part of an enzymatic complex structurally and functionally similar to *E. coli* FRD [29], depends on the chaperone SDHAF2 in conjunction with a dicarboxylate cofactor. In *Klebsiella pneumoniae,* presence of ApbE is essential for activity of its cytoplasmic fumarate reductase [20,30], suggesting a covalent attachment *in trans* by the ApbE protein. In this context, it is particularly interesting that the soluble NADH-dependent FRD in kinetoplastids [25,31], an evolutionary distant branch of eukaryotes, contains an ApbE-like domain at the N terminus of the protein. *Kinetoplastida* include pathogenic parasite species that cause major tropical diseases, such as sleeping sickness, Chagas disease or leishmaniasis. The ApbE domain is widespread in bacteria and archaea, yet only present in very few eukaryotes, notably the kinetoplastids. The model kinetoplastid *Trypanosoma brucei* encodes three NADH-dependent FRD isoforms. FRDg is localised in glycosomes, specialised peroxisome organelles harbouring glycolytic enzymes in kinetoplastids [32]. FRDm1 is localised in the mitochondrion, whereas for FRDm2 no expression or enzymatic activity was detected so far [31]. FRDg and FRDm1 are essential for a metabolic process termed succinic fermentation in the glycosomes and the mitochondrion [25]. Despite their role in maintaining the redox equilibrium by oxidation of NADH to NAD^+, none of the isoforms alone is essential for growth of the parasite in culture conditions [25,31,33].

The predicted ApbE domain of kinetoplastid FRDs is preceded by a putative flavinylation target motif (FTM; Fig. 2A,B) with a Dxx(s/t)(s/g)AS consensus sequence that slightly diverges from the prokaryotic consensus [34]. For the trypanosomatid *Leptomonas pyrrhocoris*, covalent flavin attachment at serine 9 of FRDg within the N-terminal FTM was verified by mass spectrometry [34]. Replacement of S9 by an asparagine residue abolished both flavinylation and NADH-fumarate reductase activity of FRDg upon expression in yeast. Therefore, it was suggested that the ApbE-like domain may catalyse the transfer of FMN from FAD to serine 9 of *L. pyrrhocoris* FRDg [34].

Here, we use the reverse genetic tools available for the model kinetoplastid *T. brucei* to show that the N-terminal ApbE-like domain of FRDg functions as flavin transferase *in vivo*. A minimal target sequence

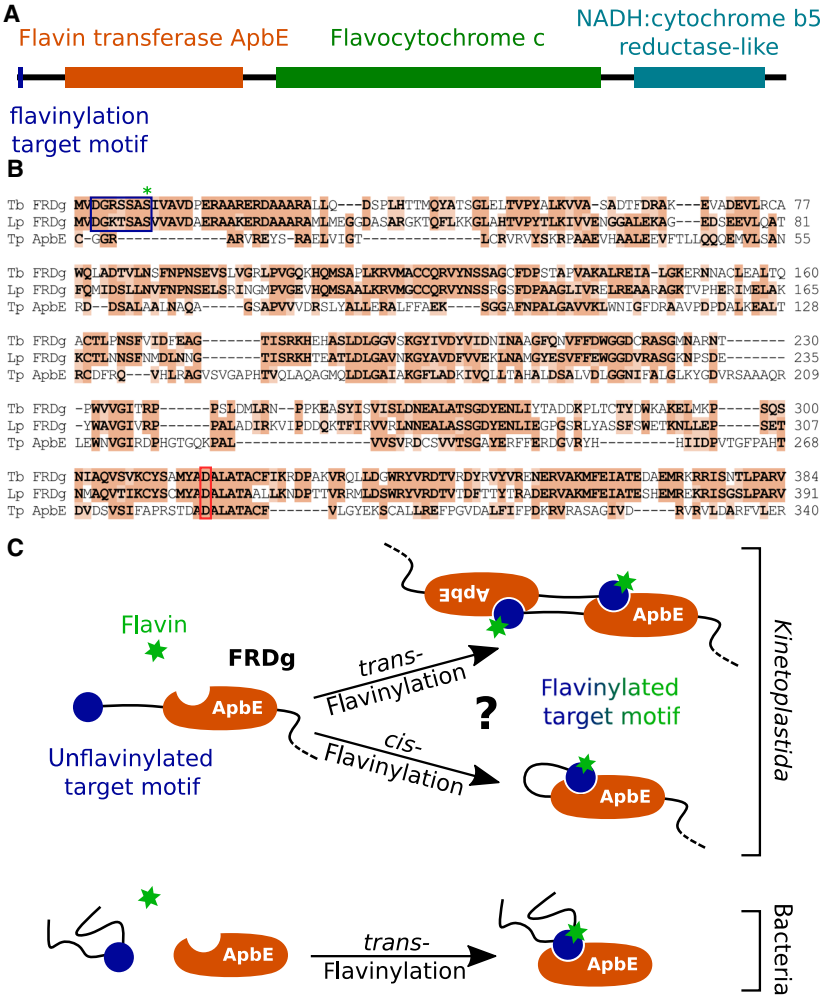

Fig. 2. Domain overview of kinetoplastid FRDg and sequence comparison with bacterial ApbE. (A) A true-to-scale representation of the *T. brucei* FRDg (TriTrypDB ID: Tb927.5.930) domain architecture as predicted by InterPro [85]. Orange box: flavin transferase ApbE domain (InterPro ID: IPR024932); green box: the flavocytochrome c domain (InterPro ID: IPR010960) that contributes the NADH:fumarate reductase catalytic centre [87]; blue box: the NADH:cytochrome b5 reductase-like domain (InterPro ID: IPR001834). (B) Protein sequence alignment of the *T. brucei* FRDg N terminus (Tb; TriTrypDB ID: Tb927.5.930), the *L. pyrrhocoris* FRDg N terminus (Lp; TriTrypDB ID: LpyrH10_01_2930) and *Treponema pallidum* ApbE (Tp; GenBank ID: AAC65759). Similar amino acids are highlighted in orange; The FTM is indicated by a blue frame, a green asterisk marking the flavin accepting Ser9 in LpFRDg. The residues aligned to Mg^{2+} binding Asp284 of TpApbE are marked by a red frame [36]. The sequence alignment was calculated with CLC Main Workbench 8.1 (https://digitalinsights.qiagen.com/) and visualised using Sequence Manipulation Suite 2 [83]. (C) Possible modes of flavinylation in different species. A model for intermolecular *trans*- and intramolecular *cis*-flavinylation by the ApbE domain of kinetoplastid FRD, compared with *trans*-flavinylation by ApbE in bacteria [18].

sufficient for flavinylation by the ApbE domain of FRD was defined that coincides with the consensus sequence. Alternative modes of ApbE-mediated flavinylation (Fig. 2C) are addressed by domain swap experiments and provide evidence for significantly higher efficiency of intramolecular *cis*-flavinylation compared with *trans*-flavinylation activity. We suggest that fusion of an ApbE domain to FRD may provide an evolutionary advantage.

Results

Flavin transferase activity of trypanosome FRDg

To trace a prominent endogenous autofluorescent band in *T. brucei* cell lines upon in-gel fluorescence analysis [35], we enriched the respective band by cell fractionation and identified it by mass spectrometry (Fig. 3) as the flavoprotein fumarate reductase (FRD). This explained the optical properties [8,9] and resistance of the fluorescence to denaturing conditions, as covalent flavin attachment to FRD had been reported in the closely related kinetoplastid *L. pyrrhocoris* [34]. The presence of an ApbE-like domain at the N terminus of FRDg led to the hypothesis of covalent FMN attachment catalysed by a eukaryotic ApbE flavin transferase activity [34]. We tested this hypothesis using the technically more amenable kinetoplastid model organism *T. brucei* that shares the domain structure and a predicted FTM Dxx(s/t)(s/g)AS with *L. pyrrhocoris*.

We first asked if the ApbE-like domain has flavin transferase activity in trypanosomes *in vivo*. The N terminus of TbFRDg with the ApbE domain and the predicted FTM and variants thereof (Fig. 4A) were transgenically expressed in *T. brucei* strain Antat1.1 90-13 and analysed in the procyclic developmental stage of the parasite. To exclude possible phenotypic effects due to expression of the truncated proteins, an inducible expression system based on the *E. coli tet* operon was used. Expression of the recombinant proteins was quantified by western blotting (Fig. 4D) using the Ty1 epitope tag. Some leakiness of the inducible expression system was noticed. Covalent flavinylation was quantified by in-gel fluorescence analysis of denaturing SDS/PAGE gels. This was possible since the only prominent autofluorescent bands in wild-type cells are the fumarate reductases FRDg and FRDm1 (Fig. 4C). The expressed ApbE domain lacks the C-terminal glycosomal targeting signal of FRDg, resulting in cytoplasmic localisation of the truncated protein (Fig. 4B). The endogenous FRDg is glycosomal and FRDm1 is mitochondrial, due to their C-terminal and N-terminal topogenic signals, respectively [31]. Therefore, we excluded significant flavinylation of the transgenically expressed truncated proteins by the endogenous FRD paralogues that both contain predicted ApbE domains.

FRDg(1-363) encompassing the FTM and the ApbE domain was covalently flavinylated (Fig. 4C; band at 46 kDa). Replacement of Ser9, the flavin accepting residue in the orthologous *L. pyrrhocoris* FRD, with asparagine had abolished flavinylation [34] (Fig. 4C). We used the same replacement in *T. brucei* (FRDg(1-363)-S9N) to confirm that Ser9 in the target motif DGRSSAS is the acceptor residue. The aspartic acid

A

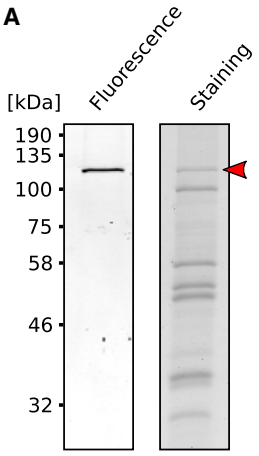

B

Protein Name	TriTrypDB Accession	Peptide Count	MS/MS Count	Intensity	iBAQ
NADH-dependent fumarate reductase	Tb927.5.930 Tb11.v5.0613.1 Tb927.5.940 Tb927.10.3650	42 26 17 1	82	3 376 300 000	54 456 000
hypothetical protein, conserved	Tb927.3.4590	1	1	24 146 000	1 724 700
hypothetical protein, conserved	Tb927.5.3470	1	1	23 352 000	1 668 000

Fig. 3. (A) In-gel fluorescence analysis (left) and matched Coomassie staining (right) of a partially purified fraction of procyclic cell lysates. The excised band (marked by a red arrow) was destained, digested with trypsin and analysed by a LC MS/MS run and MALDI-TOF measurement. (B) Table of the top hits identified by mass spectrometry. MAXQUANT [80] software was used.

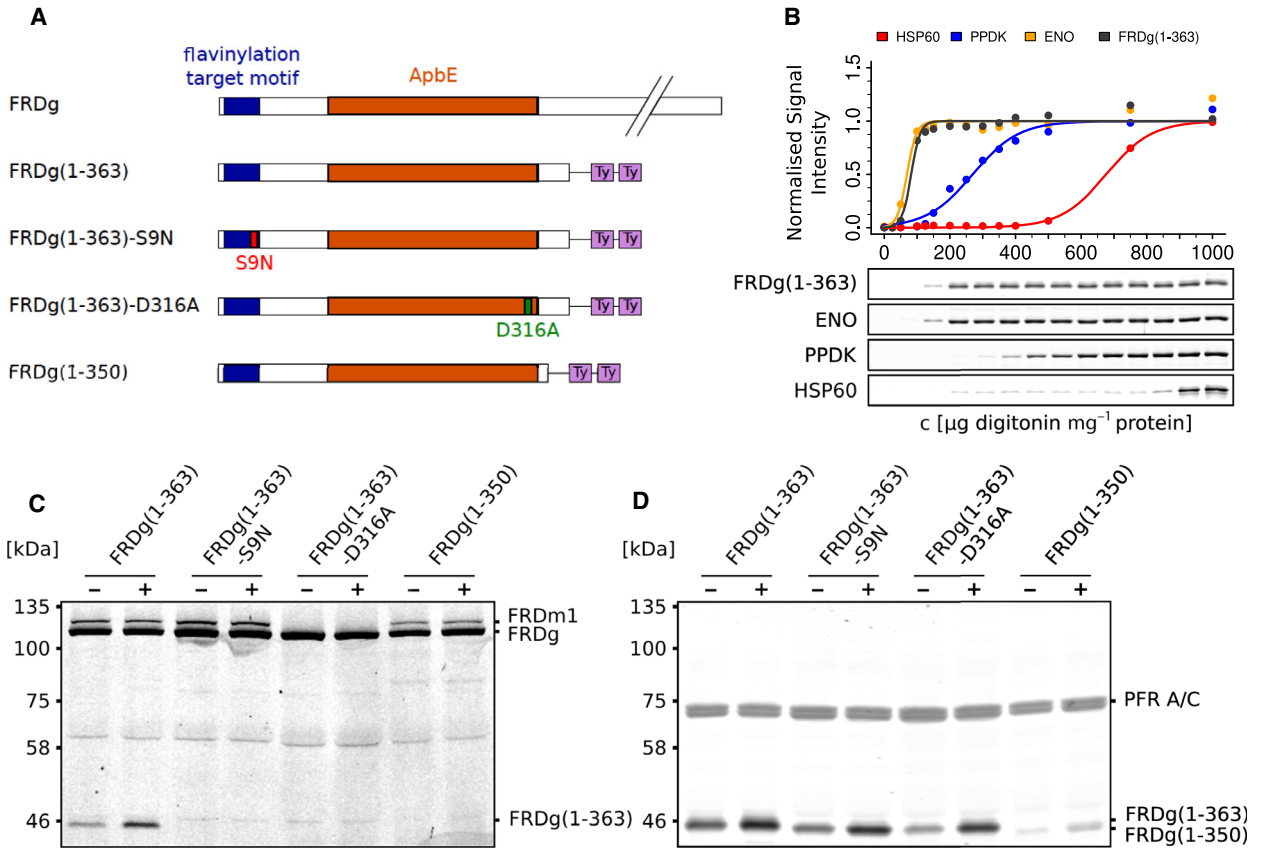

Fig. 4. Flavinylation by the eukaryotic ApbE domain *in vivo*. (A) Schematic overview of transfected C-terminal TbFRDg truncation constructs, all Ty1-tagged at the C terminus. Wild-type FRDg is shown as reference. The ApbE domain is indicated as orange box. The FTM is shown as blue box; the Ser9 to Asn mutation is highlighted in red, and the Asp316 to Ala mutation is marked in green. The Ty1 epitopes are highlighted in light purple. (B) Subcellular localisation of FRDg(1-363) by digitonin fractionation. Mitochondrial (α-HSP60), cytoplasmic (α-ENO) and glycosomal (α-PPDK) markers were compared with FRDg(1-363) (α-Ty1). Normalised signal intensities were plotted against the respective digitonin concentration. (C) In-gel fluorescence analysis for detection of covalently bound flavins in procyclic cell lines as indicated; (–) not induced, (+) tet-induced. The FRDm1 band is not visible in the FRDg(1-363)-D316A cell line, as the parental AnTat1.1 90-13 clone showed declining expression of endogenous FRDm1, prior to this transfection. (D) Western blot corresponding to C. α-Ty1 was used for detection of FRDg truncations; α-PFR-A/C was used as loading control. For constructs FRDg(1-363), FRDg(1-363)-S9N, FRDg(1-363)-D316A and FRDg(1-350), $n = 3$, 1, 4 and 3 independent transfected cell clones, respectively, were analysed by in-gel fluorescence and western blotting. One representative clone is displayed (C, D) together with a single digitonin fractionation of these cells (B). In addition, three independent clones of FRDg(1-382)-S9N were analysed with the same result as FRDg(1-363)-S9N.

284 of *Treponema pallidum* ApbE plays a major role in Mg^{2+} cofactor binding and is essential for flavinylation activity [36]. Comparison of the *T. brucei* FRDg N terminus with the *L. pyrrhocoris* orthologue and the well-studied bacterial *T. pallidum* ApbE protein [36,37] (Fig. 2B) shows conservation of the ADALATA sequence at position 283-289 of *T. pallidum* ApbE. Site-directed mutagenesis of the residue homologous to Asp284 in *T. pallidum* ApbE was performed to obtain a catalytically inactive ApbE domain (FRDg(1-363)-D316A). No flavinylation of this protein was detected albeit expressed at the same level as FRDg(1-363) (Fig. 4C). Truncation of the ApbE domain from the C-terminal side in FRDg(1-350) also resulted in loss of flavinylation, probably by disrupting structural integrity close to the Mg^{2+}-binding site. Lower abundance of FRDg(1-350) in four independent *T. brucei* cell lines, compared with FRDg(1-363), is compatible with reduced stability of this truncated protein (Fig. 4D showing one representative line). These results led to the conclusion that the ApbE domain of FRDg has flavinylation activity and catalyses autoflavinylation of the FRDg N-terminal motif. In addition, the activity does not depend on the glycosomal environment where

FRDg is naturally localised, as FRDg(1-363) is expressed in the cytoplasm. Whether the autoflavinylation proceeds as intramolecular or intermolecular reaction cannot be determined from the experiment (Fig. 2C).

Trans-flavinylation of a 37 AA acceptor fragment is catalysed by the ApbE domain of FRDg

Next, we aimed at defining the minimal fragment sufficient to serve as flavinylation acceptor in a heterologous protein context. The first 37 amino acids of FRDg were fused to aconitase (ACO) devoid of the N-terminal mitochondrial import signal (FRDg(1-37)-ACO; Fig. 5A). ACO is a dual localisation enzyme in trypanosomes [38] and, upon removal of the mitochondrial import signal, is exclusively present in the cytoplasm. FRDg(1-37)-ACO was tet-inducibly expressed in the bloodstream form (BSF) of *T. brucei* (Fig. 5D) and its subcellular localisation verified by digitonin solubilisation in procyclic cells differentiated from a FRDg(1-37)-ACO expressing BSF clone (Fig. 5B). As expected, no flavinylation of FRDg(1-37)-ACO was detected in absence of a functional ApbE protein in the same (cytoplasmic) compartment. Upon coexpression of FRDg(1-363), the FRDg(1-37)-ACO fusion protein became flavinylated, as evidenced by a fluorescent band at the expected size of the fusion protein (Fig. 5C). Autoflavinylation of FRDg(1-363) was at the same level compared with the control expressing

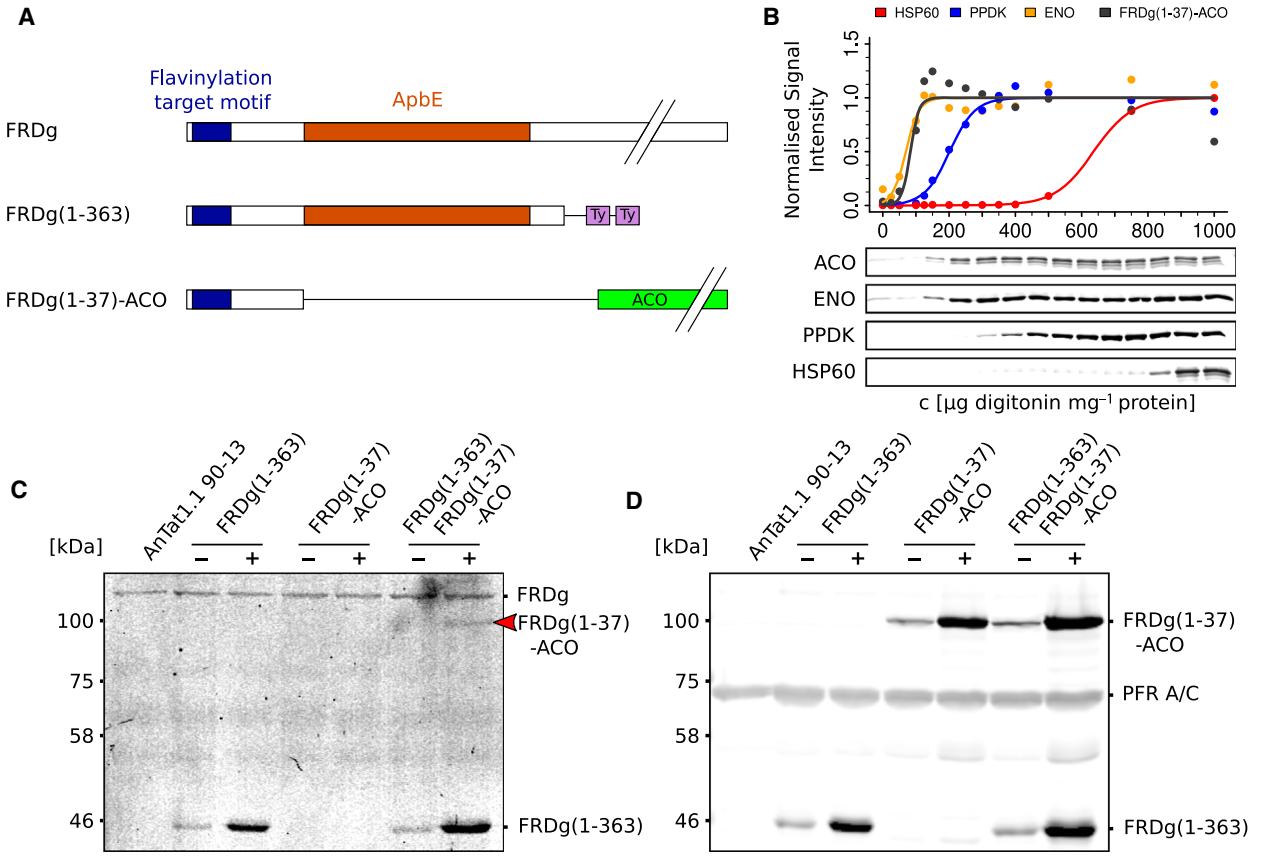

Fig. 5. ApbE domain-mediated *trans*-flavinylation of a small FTM-containing FRDg-peptide. (A) Schematic overview of transfected constructs FRDg(1-363) and FRDg(1-37) fused to cytoplasmic ACO (FRDg(1-37)-ACO). FRDg(1-363) is Ty1-tagged at the C terminus. The ACO coding region is highlighted in green, the Ty1 epitopes in light purple. (B) Digitonin fractionation showing cytoplasmic localisation of FRDg(1-37)-ACO in procyclic *T. brucei*. Rat α-ACO was used for detection of FRDg(1-37)-ACO, for marker proteins see legend to Fig. 4B. (C) In-gel fluorescence for detection of covalently bound flavins in BSF *T. brucei* expressing FRDg(1-37)-ACO (marked by a red arrow) or FRDg(1-363) or both; (–) not induced, (+) tet-induced. FRDm1 is expressed at levels below detection limit in BSF [31]. (D) Western blot corresponding to C. α-Ty1 was used for detection of FRDg(1-363), rabbit α-ACO was used for detection of FRDg(1-37)-ACO, and α-PFR-A/C was used as loading control. For constructs FRDg(1-363), FRDg(1-37)-ACO and FRDg(1-363)/FRDg(1-37)-ACO $n = 3$, 2 and 4 independent transfected cell clones, respectively, were analysed by in-gel fluorescence and western blotting. One representative clone is displayed (C, D) together with a single digitonin fractionation of these cells (B).

FRDg(1-363) alone. We can draw four conclusions from these results: (a) there is no detectable, endogenous flavin transferase in the cytoplasm, (b) the first 37 amino acids of FRDg are sufficient to serve as flavinylation acceptor, (c) the predicted ApbE domain of FRDg is a functional flavin transferase, independently confirming evidence in Fig. 4, and (d) the ApbE domain of FRDg is able to *trans*-flavinylate a target motif *in vivo*, as reported for bacterial ApbEs.

Intramolecular *cis*-flavinylation of FRDg is more efficient

Since the ApbE domain in FRDg is able to flavinylate substrates *in trans* in the same way as bacterial ApbE enzymes, but is physically linked to its major substrate in the same polypeptide chain, alternative mechanisms of autoflavinylation depicted in Fig. 2C are possible: (a) *trans*-flavinylation of FRDg(1-363) by another FRDg(1-363) polypeptide or (b) intramolecular *cis*-flavinylation. We designed cell lines to compare *in vivo* the efficiency of both reactions. To test this in a physiologically relevant context, we fused the ApbE domain FRDg(1-363), its catalytically inactive variant FRDg (1-363)-D316A and N-terminal fragments only containing the FTM to glycosomally localised isocitrate dehydrogenase (constructs FRDg(1-363)-IDHg, FRDg (1-363)-D316A-IDHg, FRDg(1-37)-IDHg, FRDg(1-9)-IDHg; Fig. 6A). In the resulting transgenic cell lines, the glycosomal environment was maintained and *in vivo*-like concentration of enzyme and peptide substrate were ensured (Fig. 6B). Targeting of all fusion proteins to the glycosome was verified by digitonin fractionation (Fig. 6C–F), and equivalent expression levels are documented in Fig. 6B. The endogenous FRDg was present as internal reference and active flavin transferase in the glycosomes of all transgenic lines (Fig. 6B). The flavinylation efficiency was expressed as ratio between covalent flavin attachment detected by direct in-gel fluorescence (Fig. 7B,D,F) and the expression level of the fusion protein quantified by western blotting using an IDHg-specific antibody (Fig. 7C,E, G). In addition, we normalised to the total amount of active flavin transferase in the glycosomes co-expressing FRDg(1-363)-IDHg and endogenous FRDg. The data from multiple independent experiments are displayed in Fig. 7. The results clearly show a much stronger flavinylation of FRDg(1-363)-IDHg compared with the catalytically inactive, but otherwise identical FRDg(1-363)-D316A-IDHg variant that is unable to execute the intramolecular reaction (Figs 6B and 7A). We conclude that the intramolecular *cis*-flavinylation is 5× more efficient, this being a minimal estimate. The unusual fusion of the ApbE domain to its substrate FRD may provide a selective advantage during rapid metabolic adaptation of trypanosomes. The degree of *trans*-flavinylation of FRDg(1-37)-IDHg and FRDg(1-363)-D316A-IDHg by the endogenous FRDg is very similar, showing that the N-terminal 37 amino acids are fully sufficient as flavinylation target. This quantitatively confirms the independent results in Fig. 5. In contrast, flavinylation of FRDg(1-9)-IDHg was not detected (Fig. 6B). Apparently, the residues or the sequence environment C-terminal to the minimal consensus motif are also important.

Discussion

This work shows that the ApbE-like domain present at the N terminus of FRD of the kinetoplastid parasite *T. brucei* has flavin transferase activity *in vivo*. ApbE-like domains are present in very few eukaryotic taxa, and here, functional activity of the predicted flavin transferase is documented for the first time to the best of our knowledge. To measure the activity *in vivo,* we used transgenic expression in the cytoplasm, a subcellular compartment devoid of measurable flavin transferase activity, and quantified direct in-gel fluorescence of flavin covalently attached to the transgenic substrate. The specificity of the reaction was dually controlled by a catalytically inactive variant of the enzyme and by separate expression of the ApbE domain and

Fig. 6. Flavinylation of the FRDg N terminus in glycosomes. (A) Transfected IDHg-fusion constructs with IDHg coding region highlighted in turquoise; see legend to Fig. 4A. (B) In-gel fluorescence (upper panel) and corresponding western blot (lower panel) for detection of covalently bound flavins in procyclic cell lines constitutively expressing the fusion proteins listed in A. α-IDHg was used for detection of the fusion proteins, and α-PFR-A/C was used as loading control. The following abbreviations were used: 9-IDHg for FRDg(1-9)-IDHg, 37-IDHg for FRDg(1-37)-IDHg, 363-IDHg for FRDg(1-363)-IDHg. (C-F) Glycosomal localisation of FRDg(1-9)-IDHg (C), FRDg(1-37)-IDHg (D), FRDg(1-363)-IDHg (E), and FRDg(1-363)-D316A-IDHg (F) was verified by digitonin fractionation. α-IDHg was used for detection of the fusion proteins, controls as detailed in legend to Fig. 4B. In D data points for digitonin concentrations > 400 $\mu g \cdot mg^{-1}$ were omitted as outliers that interfered with the curve fitting algorithm. For constructs FRDg(1-9)-IDHg, FRDg(1-37)-IDHg, FRDg(1-363)-IDHg and FRDg(1-363)-D316A-IDHg $n = 4$, 4, 3 and 5 independent transfected cell clones, respectively, were analysed by in-gel fluorescence and western blotting. One representative clone is displayed (B) together with a single digitonin fractionation of these cells (C-F).

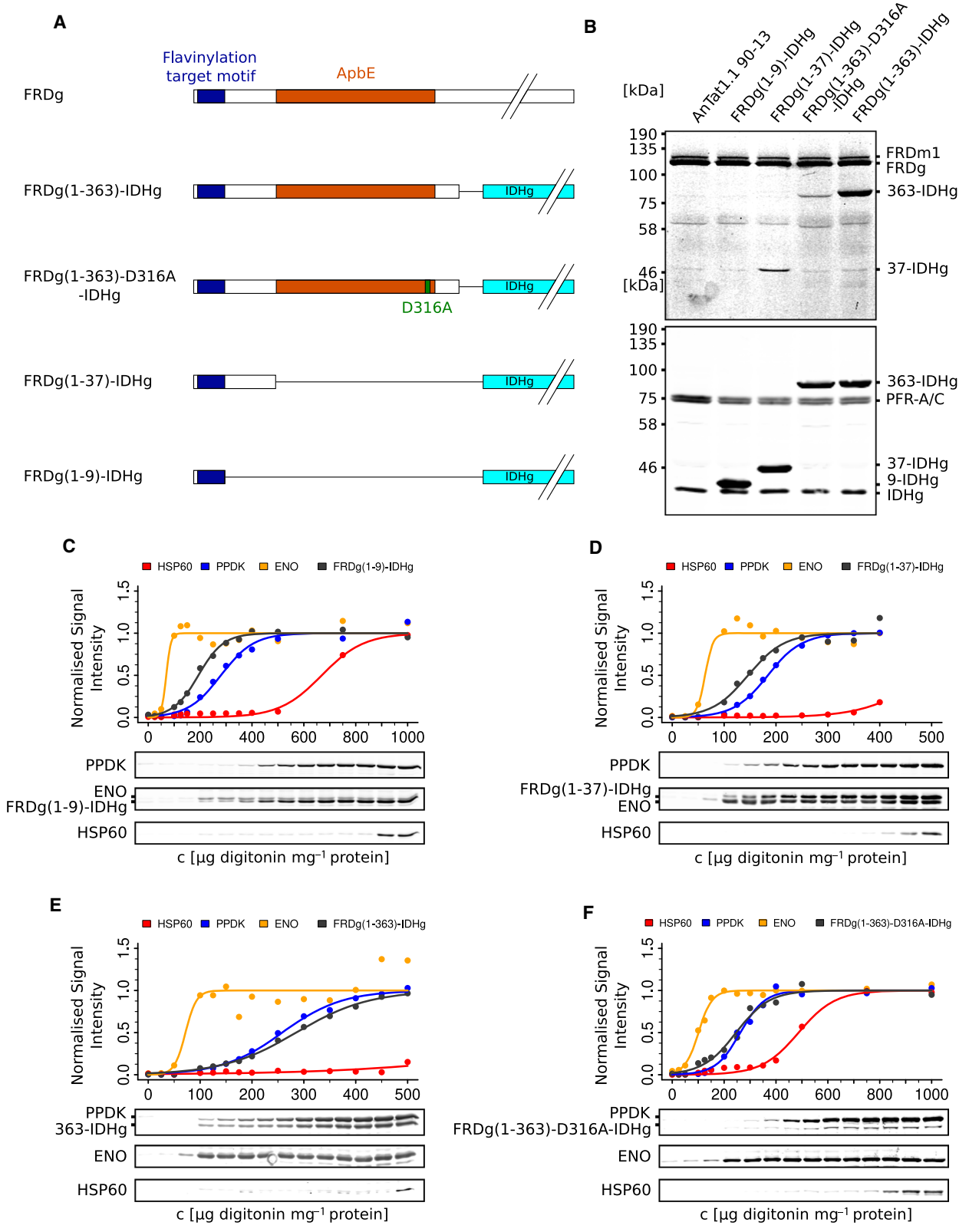
A
Flavinylation target motif
ApbE
FRDg
FRDg(1-363)-IDHg
IDHg
FRDg(1-363)-D316A -IDHg
D316A
FRDg(1-37)-IDHg
FRDg(1-9)-IDHg
B
[kDa]
AnTat1.1 90-13
FRDg(1-9)-IDHg
FRDg(1-37)-IDHg
FRDg(1-363)-D316A -IDHg
FRDg(1-363)-IDHg
190
135
100
75
58
46
FRDm1
FRDg
363-IDHg
37-IDHg
PFR-A/C
9-IDHg
IDHg
C
HSP60
PPDK
ENO
FRDg(1-9)-IDHg
Normalised Signal Intensity
c [µg digitonin mg⁻¹ protein]
D
FRDg(1-37)-IDHg
E
FRDg(1-363)-IDHg
363-IDHg
F
FRDg(1-363)-D316A-IDHg

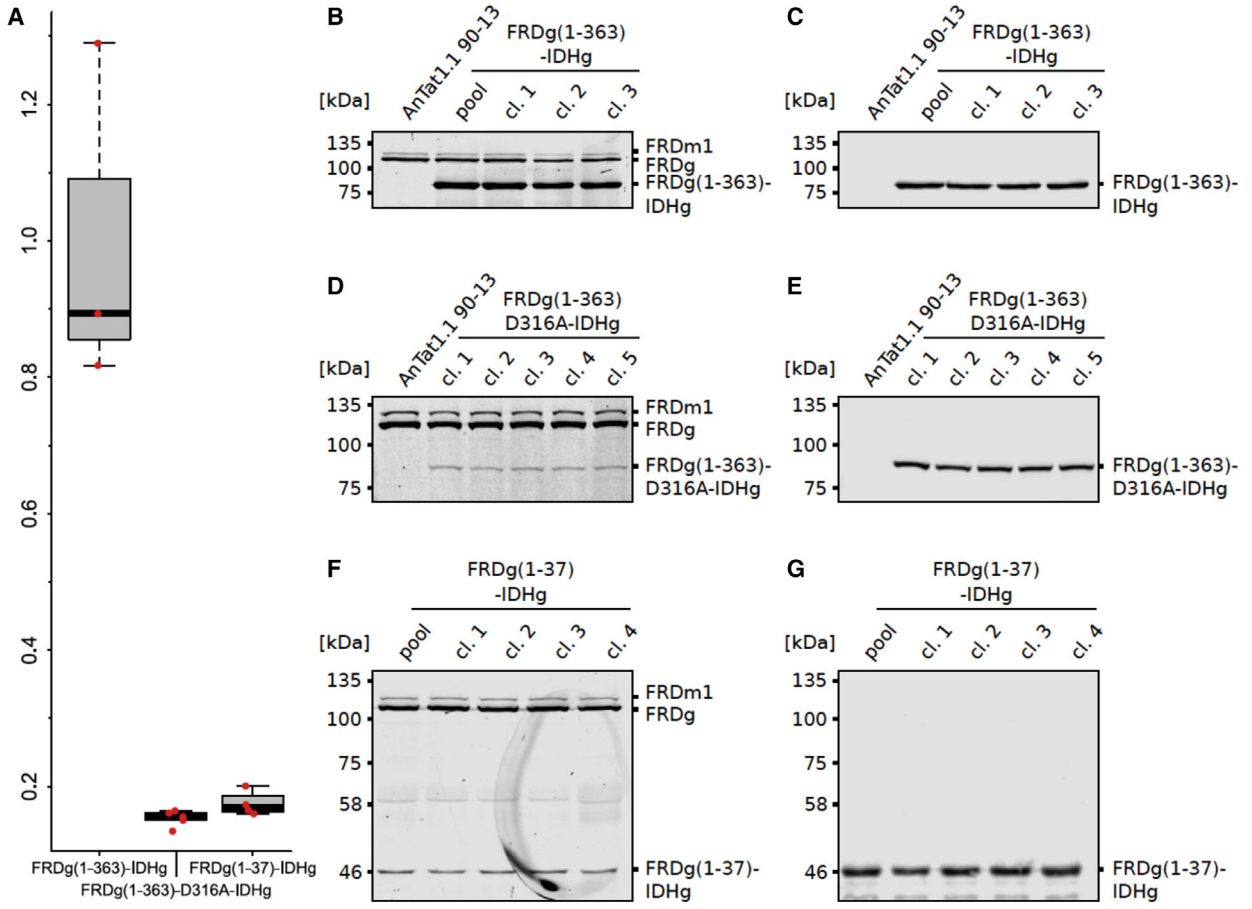

Fig. 7. In glycosomes *cis*-flavinylation of FRDg is more efficient than *trans*-flavinylation. (A) Quantification of flavinylation efficiency. The in-gel fluorescence signal of independent clonal cell lines (FRDg(1-363)-IDHg: $n = 3$; FRDg(1-363)-D316A-IDHg: $n = 5$; FRDg(1-37)-IDHg: $n = 4$; see B-G) was normalised to the protein abundance as determined by western blotting of the same gel. The mean of the FRDg(1-363)-IDHg values was set as 100%. In addition, we normalised the value for the FRDg(1-363)-IDHg cell line to the total amount of active flavin transferase in the glycosomes co-expressing FRDg(1-363)-IDHg and endogenous FRDg, using the flavin fluorescence signal. The standard box plot analysis shows median, first and third quartile of the resulting data; the whiskers define an outlier criterion at 1.5 times the interquartile range. (B) In-gel fluorescence analysis of one pool and three clonal (cl. 1-3) PCF cell lines constitutively expressing FRDg(1-363)-IDHg. (D) In-gel fluorescence analysis of five clonal (cl. 1-5) PCF cell lines constitutively expressing FRDg(1-363)-D316A-IDHg. (F) In-gel fluorescence analysis of one pool and four clonal (cl. 1-4) PCF cell lines constitutively expressing FRDg(1-37)-IDHg. (C, E, G) Western blots of the gels depicted in B, D, F, respectively; α-IDHg was used for detection. For constructs, FRDg(1-363)-IDHg, FRDg(1-363)-D316A-IDHg and FRDg(1-37)-IDHg $n = 3$, 5 and 4 independent transfected cell clones, respectively, were analysed by in-gel fluorescence and western blotting (B-G).

the flavinylation target sequence. These controls also confirmed the absence of other covalent flavinylation activities in the cytoplasm of trypanosomes. The assay was performed in the bloodstream and procyclic developmental stages (Figs 4 and 5). Although the FTM and the ApbE domain are juxtaposed in FRDg on the polypeptide chain, the ApbE domain alone is sufficient for *trans*-flavinylation of the substrate, as expected from the analogy to bacterial ApbE proteins (Fig. 5).

The N-terminal 37 amino acids of FRDg that include the Dxx(s/t)(s/g)AS consensus motif [34] are sufficient as substrate for efficient flavinylation when fused to different proteins localised in the cytoplasm or in the glycosome. We also confirmed that Ser9 in this motif is essential for flavinylation [39], in agreement with Serebryakova *et al.* [34] who detected flavin attached to this site by MS in *L. pyrrhocoris*. The minimal motif fused to a heterologous protein (FRDg(1-9)-IDHg) was, however, not sufficient. Accordingly, the first 28 amino acids of FRDg in kinetoplastids are perfectly conserved [40] (Fig. 2B) and secondary structures predicted upstream of the ApbE domain are preserved. This suggests additional structural or sequence requirements for recognition of the flavinylation target.

In bacterial Na+-translocating NADH:quinone oxidoreductase [21], a conserved leucine is present close to the consensus motif at the position aligning to valine 11 of kinetoplastid FRDg (Fig. 2B). Thus, a hydrophobic amino acid at this position might expand the minimally required motif.

Addressing the alternative mechanisms depicted in Fig. 2C, we found that *cis*-flavinylation of the FRDg target motif by the adjacent ApbE domain is at least fivefold more efficient than *trans*-flavinylation. This conclusion follows from the large quantitative difference in flavinylation efficiency of the transfected intact FRDg N terminus, compared with target proteins that only carry FRDg(1-37) or a catalytically inactive variant ApbE domain (FRDg(1-363)-D316A), all expressed in glycosomes in the presence of endogenous FRDg (Figs 6 and 7). Several arguments support validity of this conclusion: (a) all proteins were expressed at near 1 : 1 stoichiometry and at a level very close to endogenous FRDg in the native subcellular localisation in glycosomes, (b) analysis *in vivo* guarantees the physiological context, (c) the conclusion is independent of the endogenous flavinylation activity in glycosomes, that we assume to be exclusively FRDg, and (d) the assumption that full-length FRDg and FRDg(1-363) have the same specific flavinylation activity is very likely correct, as the ApbE domain is structurally independent. The higher efficiency of the *cis*-flavinylation is consistent with less limitation by substrate diffusion.

Flavoproteins have interesting properties for biotechnological applications. Flavin-based fluorescent proteins (FbFPs) are derived from light–oxygen–voltage (LOV) sensing domains, utilised by plants and bacteria as blue-light photoreceptors [41,42]. Their application as fluorescent reporters offers several advantages over GFP-like fluorescent proteins, such as oxygen-independent fluorescence [43,44], a broad functional pH range (4-11) [45] and their small size – for iLOV ~ 10 kDa [46]. Other variants, such as miniSOG, can generate reactive singlet oxygen upon illumination, which is exploited for electron microscopy [47]. Furthermore, advances in signal intensity [48] allow application in super-resolution microscopy [49]. Known FbFPs use noncovalently bound flavin as cofactor, making them prone to denaturation by elevated temperatures [45]. Although variants with increased thermal stability exist [50], covalently bound flavin can tolerate even extended periods of thermal stress in the presence of detergents as shown by the assay used here for detection of flavinylation. We propose FRDg(1-37) as heat-stable, detergent-resistant fluorescent protein tag with a size of ~ 4 kDa, which is significantly smaller than a similar system proposed by Kang *et al.* [51] that utilises *Vibrio cholerae* Na^+-translocating NADH:quinone oxidoreductase C (27 kDa) as tag in eukaryotic cells, which is flavinylated by ectopically expressed bacterial ApbE. The efficiency of the *trans*-flavinylation and sensitivity may limit general applicability as a tag for fluorescence microscopy, yet we envisage an application to analyse glycosomal import in kinetoplastids: the *trans*-flavinylation activity of endogenous glycosomally localised FRDg will be exploited to specifically detect and quantify any imported protein fused to the N-terminal FRDg(1-37) tag by direct in-gel fluorescence or flavin-specific antibodies [52] on denaturing PAGE. Only upon effective import, the tag on the fusion protein will be flavinylated *in trans* by FRDg, enabling analysis without prior cell fractionation. This N-terminal tagging approach is unlikely to interfere with the glycosomal import mechanism, which mostly relies on a C-terminal peroxisomal-targeting signal [53]. The strategy can be used to map glycosomal import sequence requirements, study the import mechanism and its regulation or screen for novel glycosomal proteins.

Eukaryotic ApbE domains are rare and limited to few clades of the tree of life. The domain architecture of kinetoplastid FRDs (Fig. 2A) is also predicted for some algal FRDs, such as *Symbiodinium microadriaticum* (GenBank ID: OLP85325), *Nannochloropsis gaditana* (GenBank ID: EWM27529) or *Nannochloropsis salina* (GenBank ID: TFJ85565). In contrast, the FRD of *Diplonema papillatum* (GenBank ID: LMZG01019705), that is in a clade close to kinetoplastids, is not linked to an ApbE domain and no distinct ApbE protein could be detected in the *D. papillatum* genome so far. Independent fusion events of an ApbE domain to FRD in those phylogenetically distant taxa are compatible with an evolutionary advantage of intramolecular FRD flavinylation in certain physiological situations. The bacterial *K. pneumoniae* FRD provides a potential example of an evolutionary intermediate, where FRD and ApbE are transcribed from a single operon, but still form distinct proteins [20,21].

Can we envisage a metabolic reason for the benefit of a more efficient *cis*-flavinylation of FRD in some organisms? Limited availability or transport of riboflavin [54] is a possibility, as trypanosomes are riboflavin auxotrophs. Most importantly, they depend on metabolic flexibility and adaptation to rapidly changing host environments in their parasitic life cycle. In the mammalian bloodstream, a simplified metabolism relies predominantly on the glucose supplied by the mammalian host. Pyruvate is the main glycolytic end product [32,55]. Upon transmission to the glucose-

depleted, amino acid-rich environment [56] in the tsetse fly insect vector, differentiation into the procyclic stage [57] results in major adaptions of the parasite's metabolism. Energy sources are partially oxidised by aerobic fermentation to acetate or succinate [32]. In the glycosomes, this is achieved by establishment of the succinic branch of glycolysis [58], where FRDg regenerates NAD^+ by reduction of fumarate to succinate [31,32,59]. To enable this rapid metabolic adaptation, glycosomes are remodelled depending on carbon source by degradation via pexophagy and *de novo* synthesis of glycosomes during differentiation of the parasite [60,61]. The fusion of an ApbE flavin transferase domain to FRD results in more efficient *cis*-flavinylation, as shown here (Fig. 7A). The intramolecular reaction may also support faster flavinylation of *de novo* synthesised FRDg even at limiting flavin concentrations. As flavinylation is a prerequisite for enzymatic activity [21], the kinetoplastid enzyme might be optimised for efficiently re-establishing FRD catalytic activity to guarantee the glycosomal redox balance upon glycosome turnover and thereby provide an increased fitness in the rapidly changing environments the parasite inhabits. The same argument may be valid for the mitochondrial isoform FRDm1, as the trypanosomal mitochondrion undergoes extreme developmental restructuring in the life cycle.

Materials and methods

T. brucei cultivation

The BSF of AnTat1.1 90-13, a pleomorphic *T. brucei brucei* cell line constitutively expressing T7 RNA polymerase and tetracycline (tet) repressor [62,63], was cultured at 37 °C and 5% CO_2 atmosphere in modified HMI-9 medium [64] containing 10% (V/V) heat-inactivated FCS. The procyclic form (PCF) was cultivated at 27 °C in modified SDM-79 medium [65] supplemented with 10% (V/V) heat-inactivated FCS, 7.5 mg·L^{-1} hemin, 10 mM glucose and 10 mM glycerol. Continuous selection was performed with hygromycin B (BSF: 2.5 μg·mL^{-1}; PCF: 25 μg·mL^{-1}), G418 (BSF: 2.0 μg·mL^{-1}; PCF: 15 μg·mL^{-1}). To differentiate BSF to PCF, cultures were started at a density of 5.0×10^5/mL. Growth was continued for 36 h without dilution. Usually, 10 mL of culture was harvested, resuspended in 5 mL modified DTM medium [64] supplemented with 6 mM cis-aconitate and continued as procyclic cultures by dilution with SDM-79 upon resuming proliferation. If not specified otherwise, enzymes were obtained from New England Biolabs (Frankfurt am Main, Germany) and other chemicals from Sigma-Aldrich (Darmstadt, Germany).

Transgenic cell lines

To express *FRDg(1-350)*, a C-terminal truncation of FRDg (TriTrypDB ID: Tb927.5.930) with a length of 350 amino acids, followed by two Ty1 epitopes [66], linked and interspaced with (PS)x1 linkers (DNA: CCAAGT), was inserted between the HindIII and BamHI restriction sites of the tet-inducible pLew82 [67] expression vector. The respective fragment was amplified from genomic DNA of strain AnTat1.1 Munich [63]. NotI was used for plasmid linearisation before transfection of the AnTat1.1 90-13 cell line with the *Nucleofector II* device (Amaxa Biosystems, Cologne, Germany) [68]. Continuous selection was performed with phleomycin (BSF: 2.0 μg·mL^{-1}; PCF: 2.5 μg·mL^{-1}).

The same approach was used to express *FRDg(1-363)*, *FRDg(1-363)-S9N* that is identical to *FRDg(1-363)* except for a substitution of serine 9 (TCA) with asparagine (AAT) and *FRDg(1-363)-D316A* that is identical to *FRDg(1-363)* except for a substitution of aspartic acid 316 (GAC) with alanine (GCA).

FRDg(1-37) was N-terminally fused to *T. brucei ACO* (TriTrypDB ID: Tb927.10.14000) [38], replacing the mitochondrial targeting signal (FRDg(1-37)-ACO). Using XbaI, two fragments were inserted simultaneously between the HindIII and BamHI restriction sites of pLew82 with a puromycin resistance cassette; (a) a fragment containing the first 111 bp of the *FRDg* gene, followed by a flexible GSAGSAAGSGEF linker [69] (DNA: GGGTCTGCGG GGTCTGCAGCTGGGAGTGGTGAGTTT), (b) a 2664 bp fragment of *ACO* position 31-2694. AnTat1.1 90-13 and the derived FRDg(1-363) cell line were transfected with the plasmid. Continuous selection was performed with puromycin (BSF: 0.1 μg·mL^{-1}; PCF: 1.0 μg·mL^{-1}).

The same approach was used to express *FRDg(1-382)-S9N* that differs from *FRDg(1-363)-S9N* by the position of the truncation and C-terminal fusion of the C-terminal 15 amino acids of FRDg. Two fragments were inserted into pLew82 with a phleomycin resistance cassette; (a) a fragment containing the first 1146 bp of the *FRDg* gene, (b) a fragment containing two Ty1 epitopes [66] and the C-terminal 45 bp of the *FRDg* gene, linked and interspaced with (PS)x1 linkers. Continuous selection was performed with phleomycin (BSF: 2.0 μg·mL^{-1} PCF: 2.5 μg·mL^{-1}).

FRDg(1-363) was N-terminally fused to glycosomal isocitrate dehydrogenase (TriTrypDB ID: Tb927.11.900), resulting in the fusion protein FRDg(1-363)-IDHg. A fragment containing the first 1089 bp of the *FRDg* gene, followed by a GSAGSAAGSGEF linker, was inserted between the HindIII and AgeI restriction sites of an *IDHg* open reading frame containing plasmid [70] based on the constitutive expression vector pTSARib [71]. BglII was used for plasmid linearisation before transfection of the AnTat1.1 90-13 cell line. Continuous selection was

performed with puromycin (BSF: 0.1 μg·mL^{-1}; PCF: 1.0 μg·mL^{-1}).

The same approach was used to express three additional FRDg-IDHg-fusion proteins: (a) *FRDg(1-9)-IDHg* (FRD (1-9) N-terminally fused to IDHg), (b) *FRDg(1-37)-IDHg* (FRD(1-37) N-terminally fused to IDHg) and (c) *FRDg(1-363)-D316A-IDHg* (FRD(1-363)-D316A N-terminally fused to IDHg).

Primer sequences are available upon request.

SDS/PAGE and western blot analysis

Cells were washed in PBS and resuspended to 3.0×10^5/μL in Laemmli sample buffer [58.33 mM Tris/HCl (pH 6.8); 200 mM DTT; 5% (V/V) glycerol; 1.71% (m/V) SDS; 0.002% (m/V) bromophenol blue; solvent: H_2O]. After incubation at 95 °C for 5 min, the sample was sonicated three times for 30 s on/off with a *Bioruptor* (Diagenode SA, Seraing, Belgium) on high power. Ten microlitre of the sample was subjected to SDS/PAGE (8% or 10%). Western blotting was performed onto a polyvinylidene fluoride membrane with the *Trans-Blot Turbo Transfer System* (Bio-Rad Laboratories, Feldkirchen, Germany). Mouse α-PFR-A/C (clone: L13D6; 1 : 2000) [72], mouse α-Ty1 (clone: BB2; 1 : 500) [66], rabbit α-IDHg (1 : 5000) [70], rabbit α-ACO (1 : 750) [73], rat α-ACO (1 : 750) [73], rabbit α-PPDK (1 : 1000) [74], mouse α-HSP60 (1 : 5000) [75,76] and rabbit α-ENO (1 : 100 000; P. Michels, Edinburgh, UK) were used as primary antibodies for immunodetection. For near-infrared fluorescence detection, goat IR-BLOT 800 α-mouse IgG (1 : 5000; Cyanagen Srl, Bologna, Italy) or goat IRDye 800CW α-mouse IgG (H + L) (1 : 5000; LI-COR Bioscience, Bad Homburg, Germany), goat IRDye 800CW α-rat IgG (H + L) (1 : 5000; LI-COR Bioscience) and goat IRDye 680LT α-rabbit IgG (H + L) (1 : 5000; LI-COR Bioscience) were used as secondary antibodies. Image acquisition was performed with the Odyssey CLx Near-Infrared Fluorescence Imaging System (LI-COR Bioscience).

Flavinylation analysis by in-gel fluorescence

As described before [35], SDS/PAGE gels were scanned with a Typhoon TRIO Variable Mode Imager System (GE Healthcare, Solingen, Germany). λ_{ex} = 488 nm and λ_{em} = 526 nm were used for detection of covalently bound flavin and λ_{ex} = 670 nm and λ_{em} = 633 nm for visualisation of the Blue Prestained Protein Standard (New England Biolabs).

Subcellular digitonin fractionation

2.0×10^9 procyclic *T. brucei* cells were harvested and washed twice in PBS. The cells were resuspended to 6.5×10^8/mL in STEN buffer [250 mM sucrose; 150 mM NaCl; 25 mM Tris/HCl (pH 7.4); 1 mM EDTA] supplemented with 3.5% (V/V) PMSF (57 mM; solvent: isopropanol). Two hundred microlitre of aliquots of the cell suspension (corresponding to 660 μg protein [77]) was incubated for 4 min at 25 °C in 14 different digitonin concentrations. Immediately after incubation, the samples were centrifuged at 14 000 ***g*** for 2 min. The supernatant was analysed by SDS/PAGE and western blotting. Pyruvate phosphate dikinase (PPDK), heat-shock protein 60 (HSP60) and enolase (ENO) were used as glycosomal, mitochondrial and cytoplasmic marker proteins, respectively. The maximum signal intensity obtained for each analysed protein was set to 1 and the data points were fitted to the logistic function $f(x) = A/(1+\exp((x-m)/s))$ by application of the Levenberg–Marquardt algorithm for nonlinear least-square analysis. Therefore, the Java library least-squares-in-java 1.0.1 (https://github.com/odinsbane/least-squares-in-java) was used. The initial parameter estimates were set as (A = 10, m = 250, s = 10). The data were further normalised to the respective inferred upper asymptote A for graphical representation.

Partial purification and protein identification

2.0×10^9 procyclic *T. brucei* cells of AnTat1.1E Paris [63] were harvested and washed two times in PBS. The cells were resuspended in 2.4 mL hypotonic lysis buffer [5 mM Tris/HCl (pH 7.4); 1.995 mM PMSF] and incubated 20 min on ice. All centrifugations were performed at 4 °C. Samples were centrifuged for 15 min at 1500 ***g***. The supernatant was subsequently centrifuged for 15 min at 3000 ***g***. The pellet resulting from the last centrifugation step was washed with 500 μL hypotonic lysis buffer by centrifugation at 3000 ***g*** for 15 min. The supernatant was discarded. After resuspension in hypotonic lysis buffer, centrifugation at 20 000 ***g*** for 15 min was performed. The pellet was washed in 100 μL hypotonic lysis buffer and was resuspended in 30 μL Laemmli sample buffer. Fifteen microlitres was subjected to SDS/PAGE. The gel was stained with Colloidal Coomassie Brilliant Blue G-250 [78,79]. The partially purified protein band was identified by in-gel fluorescence, excised (Fig. 3A) and destained, followed by in-gel trypsin digestion. Isolated peptides were purified using C18 stage tips and analysed by LC-MS/MS. Proteomic analysis was performed at the Protein Analysis Unit (ZfP) of the Ludwig Maximilian University of Munich, a registered research infrastructure of the Deutsche Forschungsgemeinschaft (DFG, RI-00089). MAXQUANT (www.maxquant.org) [80] software was used for peptide identification and quantification.

Bioinformatic analysis and toolchain

For statistical analysis and plotting, R 3.6.2 [81] was used with the integrated development environment RStudio 1.1.463 [82]. *In silico* cloning and sequence alignment were

performed with CLC Main Workbench 8.1 (https://digitalinsights.qiagen.com/). Sequence similarity was visualised using Sequence Manipulation Suite 2 [83]. Image postprocessing was carried out with Fiji [84], quantification with Image Studio Lite (https://www.licor.com). Protein domains were annotated and predicted using InterPro [85], while general genomic information was retrieved from TriTrypDB [40] or GenBank [86].

Acknowledgements

We thank M. Wirth, I. Forné and A. Imhof (BMC, Ludwig-Maximilians-University Munich) for the mass spectrometry service, R. Erdmann (Ruhr-University Bochum) for discussion on glycosomal import, and D. Inaoka (NEKKEN, Nagasaki University) for critical reading of the manuscript. This work was supported by the Lehre@LMU undergraduate research award (RS) and the BioNa junior scientist award of the Faculty of Biology (SB).

Conflict of interest

The authors declare no conflict of interest.

Author contributions

RS, SB and MB designed research; RS performed research; RS, SB, FB and MB analysed data; RS and MB wrote the paper.

Peer Review

The peer review history for this article is available at https://publons.com/publon/10.1111/febs.15812.

References

1 Fraaije MW & Mattevi A (2000) Flavoenzymes: diverse catalysts with recurrent features. *Trends Biochem Sci* **25**, 126–132.
2 Walsh CT & Wencewicz TA (2013) Flavoenzymes: versatile catalysts in biosynthetic pathways. *Nat Prod Rep* **30**, 175–200.
3 Zhang M, Wang L & Zhong D (2017) Photolyase: dynamics and electron-transfer mechanisms of DNA repair. *Arch Biochem Biophys* **632**, 158–174.
4 Fujisawa T & Masuda S (2017) Light-induced chromophore and protein responses and mechanical signal transduction of BLUF proteins. *Biophys Rev* **10**, 327–337.
5 Conrad KS, Manahan CC & Crane BR (2014) Photochemistry of flavoprotein light sensors. *Nat Chem Biol* **10**, 801–809.
6 Brodl E, Winkler A & Macheroux P (2018) Molecular mechanisms of bacterial bioluminescence. *Comput Struct Biotechnol J* **16**, 551–564.
7 Kao YT, Saxena C, He TF, Guo L, Wang L, Sancar A & Zhong D (2008) Ultrafast dynamics of flavins in five redox states. *J Am Chem Soci* **130**, 13132–13139.
8 Ghisla S, Massey V, Lhoste JM & Mayhew SG (1974) Fluorescence and optical characteristics of reduced flavines and flavoproteins. *Biochemistry* **13**, 589–597.
9 Ortega E, de Marcos S, Sanz-Vicente I, Ubide C, Ostra M, Vidal M & Galbán J (2016) Fluorescence of the Flavin group in choline oxidase. Insights and analytical applications for the determination of choline and betaine aldehyde. *Talanta* **147**, 253–260.
10 Fujiyoshi S, Hirano M, Matsushita M, Iseki M & Watanabe M (2011) Structural change of a cofactor binding site of flavoprotein detected by single-protein fluorescence spectroscopy at 1.5 k. *Phys Rev Lett* **106**, 078101.
11 Huijbers MME, Martínez-Júlvez M, Westphal AH, Delgado-Arciniega E, Medina M & van Berkel WJH (2017) Proline dehydrogenase from *Thermus thermophilus* does not discriminate between FAD and FMN as cofactor. *Sci Rep* **7**, 43880.
12 Miranda-Lorenzo I, Dorado J, Lonardo E, Alcala S, Serrano AG, Clausell-Tormos J, Cioffi M, Megias D, Zagorac S, Balic A *et al.* (2014) Intracellular autofluorescence: a biomarker for epithelial cancer stem cells. *Nat Methods* **11**, 1161–1169.
13 Eckers E & Deponte M (2012) No Need for labels: the autofluorescence of *Leishmania tarentolae* mitochondria and the necessity of negative controls. *PLoS One* **7**, e47641.
14 Massey V (1994) Activation of molecular oxygen by flavins and flavoproteins. *J Biol Chem* **269**, 22459–22462.
15 Macheroux P, Kappes B & Ealick SE (2011) Flavogenomics - a genomic and structural view of flavin-dependent proteins. *FEBS J* **278**, 2625–2634.
16 Starbird CA, Maklashina E, Cecchini G & Iverson TM (2015) Flavoenzymes: covalent versus noncovalent. In eLS, pp. 1–11. John Wiley & Sons, Ltd, Chichester, UK.
17 Heuts DPHM, Scrutton NS, McIntire WS & Fraaije MW (2009) What's in a covalent bond? On the role and formation of covalently bound flavin cofactors. *FEBS J* **276**, 3405–3427.
18 Bertsova YV, Fadeeva MS, Kostyrko VA, Serebryakova MV, Baykov AA & Bogachev AV (2013) Alternative pyrimidine biosynthesis protein ApbE is a flavin transferase catalyzing covalent attachment of FMN to a threonine residue in bacterial flavoproteins. *J Biol Chem* **288**, 14276–14286.
19 Deka RK, Brautigam CA, Liu WZ, Tomchick DR & Norgard MV (2015) Molecular insights into the

enzymatic diversity of flavin-trafficking protein (Ftp; formerly ApbE) in flavoprotein biogenesis in the bacterial periplasm. *MicrobiologyOpen* **5**, 21–38.
20 Bertsova YV, Kostyrko VA, Baykov AA, Bogachev AV (2014) Localization controlled specificity of FAD: threonine flavin transferases in *Klebsiella pneumoniae* and its implications for the mechanism of Na+-translocating NADH:quinone oxidoreductase. *Biochim Biophys Acta* **1837**, 1122–1129.
21 Bertsova YV, Serebryakova MV, Anashkin VA, Baykov AA & Bogachev AV (2019) Mutational analysis of the flavinylation and binding motifs in two protein targets of the flavin transferase ApbE. *FEMS Microbiol Lett* **366**, fnz252.
22 Verkhovsky MI & Bogachev AV (2010) Sodium-translocating NADH:quinone oxidoreductase as a redox-driven ion pump. *Biochim Biophys Acta*. **1797**, 738–746.
23 Van Hellemond JJ & Tielens AG (1994) Expression and functional properties of fumarate reductase. *Biochem J* **304** (Pt 2), 321–331.
24 Cecchini G, Schröder I, Gunsalus RP & Maklashina E (2002) Succinate dehydrogenase and fumarate reductase from *Escherichia coli*. *Biochim Biophys Acta* **1553**, 140–157.
25 Besteiro S, Biran M, Biteau N, Coustou V, Baltz T, Canioni P & Bringaud F (2002) Succinate secreted by *Trypanosoma brucei* is produced by a novel and unique glycosomal enzyme, NADH-dependent fumarate reductase. *J Biol Chem* **277**, 38001–38012.
26 Bamford V, Dobbin PS, Richardson DJ & Hemmings AM (1999) Open conformation of a flavocytochrome c3 fumarate reductase. *Nat Struct Biol* **6**, 1104–1107.
27 Starbird CA, Maklashina E, Sharma P, Qualls-Histed S, Cecchini G & Iverson TM (2017) Structural and biochemical analyses reveal insights into covalent flavinylation of the *Escherichia coli* Complex II homolog quinol:fumarate reductase. *J Biol Chem* **292**, 12921–12933.
28 Sharma P, Maklashina E, Cecchini G & Iverson TM (2018) Crystal structure of an assembly intermediate of respiratory Complex II. *Nat Commun* **9**, 1–11.
29 Sharma P, Maklashina E, Cecchini G & Iverson TM (2020) The roles of SDHAF2 and dicarboxylate in covalent flavinylation of SDHA, the human complex II flavoprotein. *Proc Natl Acad Sci USA* **117**, 23548–23556.
30 Bogachev AV, Baykov AA & Bertsova YV (2018) Flavin transferase: the maturation factor of flavin-containing oxidoreductases. *Biochem Soc Trans* **46**, 1161.
31 Coustou V, Besteiro S, Rivière L, Biran M, Biteau N, Franconi JM, Boshart M, Baltz T & Bringaud F (2005) A mitochondrial NADH-dependent fumarate reductase involved in the production of succinate excreted by procyclic *Trypanosoma brucei*. *J Biol Chem* **280**, 16559–16570.
32 Michels PAM, Bringaud F, Herman M & Hannaert V (2006) Metabolic functions of glycosomes in trypanosomatids. *Biochim Biophys Acta* **1763**, 1463–1477.
33 Coustou V, Biran M, Besteiro S, Rivière L, Baltz T, Franconi J-M & Bringaud F (2006) Fumarate is an essential intermediary metabolite produced by the procyclic *Trypanosoma brucei*. *J Biol Chem* **281**, 26832–26846.
34 Serebryakova MV, Bertsova YV, Sokolov SS, Kolesnikov AA, Baykov AA & Bogachev AV (2018) Catalytically important flavin linked through a phosphoester bond in a eukaryotic fumarate reductase. *Biochimie* **149**, 34–40.
35 Chiasson D, Giménez-Oya V, Bircheneder M, Bachmaier S, Studtrucker T, Ryan J, Sollweck K, Leonhardt H, Boshart M, Dietrich P *et al*. (2019) A unified multi-kingdom Golden Gate cloning platform. *Sci Rep* **9**, 10131.
36 Deka RK, Brautigam CA, Liu WZ, Tomchick DR & Norgard MV (2015) Evidence for posttranslational protein flavinylation in the syphilis spirochete *Treponema pallidum*: structural and biochemical insights from the catalytic core of a periplasmic flavin-trafficking protein. *MBio* **6**, e00519-15.
37 Deka RK, Brautigam CA, Liu WZ, Tomchick DR & Norgard MV (2013) The TP0796 Lipoprotein of *Treponema pallidum* is a bimetal-dependent FAD pyrophosphatase with a potential role in flavin homeostasis. *J Biol Chem* **288**, 11106–11121.
38 Ziebart NE (2016) Metabolic signals and pathways in development of *Trypanosoma brucei*. Thesis, Ludwig-Maximilians-Universität München, Germany.
39 Wargnies M, Plazolles N, Schenk R, Villafraz O, Dupuy JW, Biran M, Bachmaier S, Baudouin H, Clayton C, Boshart M *et al*. (2020) Metabolic selection of a homologous recombination mediated loss of glycosomal fumarate reductase in *Trypanosoma brucei*. *bioRxiv*, p. 2020.11.29.403048. "[PREPRINT]"
40 Aslett M, Aurrecoechea C, Berriman M, Brestelli J, Brunk BP, Carrington M, Depledge DP, Fischer S, Gajria B, Gao X *et al*. (2010) TriTrypDB: a functional genomic resource for the Trypanosomatidae. *Nucleic Acids Res* **38**, D457–D462.
41 Wingen M, Potzkei J, Endres S, Casini G, Rupprecht C, Fahlke C, Krauss U, Jaeger KE, Drepper T & Gensch T (2014) The photophysics of LOV-based fluorescent proteins-new tools for cell biology. *Photochem Photobiol Sci* **13**, 875–883.
42 Péresse T & Gautier A (2019) Next-generation fluorogen-based reporters and biosensors for advanced bioimaging. *Int J Mol Sci* **20**, 24.

43 Walter J, Hausmann S, Drepper T, Puls M, Eggert T & Dihné M (2012) Flavin mononucleotide-based fluorescent proteins function in mammalian cells without oxygen requirement. *PLoS One* **7**, e43921.

44 Chia HE, Marsh ENG & Biteen JS (2019) Extending fluorescence microscopy into anaerobic environments. *Curr Opin Chem Biol* **51**, 98–104.

45 Mukherjee A, Walker J, Weyant KB & Schroeder CM (2013) Characterization of flavin-based fluorescent proteins: an emerging class of fluorescent reporters. *PLoS One* **8**, 5.

46 Chapman S, Faulkner C, Kaiserli E, Garcia-Mata C, Savenkov EI, Roberts AG, Oparka KJ & Christie JM (2008) The photoreversible fluorescent protein iLOV outperforms GFP as a reporter of plant virus infection. *Proc Natl Acad Sci USA* **105**, 20038–20043.

47 Shu X, Lev-Ram V, Deerinck TJ, Qi Y, Ramko EB, Davidson MW, Jin Y, Ellisman MH & Tsien RY (2011) A Genetically encoded tag for correlated light and electron microscopy of intact cells, tissues, and organisms. *PLoS Biol* **9**, 4.

48 Mukherjee A, Weyant KB, Walker J & Schroeder CM (2012) Directed evolution of bright mutants of an oxygen-independent flavin-binding fluorescent protein from *Pseudomonas putida*. *J Biol Eng* **6**, 20.

49 Gregor C, Sidenstein SC, Andresen M, Sahl SJ, Danzl JG & Hell SW (2018) Novel reversibly switchable fluorescent proteins for RESOLFT and STED nanoscopy engineered from the bacterial photoreceptor YtvA. *Sci Rep* **8**, 2724.

50 Nazarenko VV, Remeeva A, Yudenko A, Kovalev K, Dubenko A, Goncharov IM, Kuzmichev P, Rogachev AV, Buslaev P, Borshchevskiy V *et al.* (2019) A thermostable flavin-based fluorescent protein from *Chloroexus aggregans*: a framework for ultra-high resolution structural studies. *Photochem Photobiol Sci* **18**, 1793–1805.

51 Kang MG, Park J, Balboni G, Lim MH, Lee C & Rhee HW (2017) Genetically encodable bacterial flavin transferase for fluorogenic protein modification in mammalian cells. *ACS Synth Biol* **6**, 667–677.

52 Barber MJ, Eichler DC, Solomonson LP & Ackrell BA (1987) Anti-flavin antibodies. *Biochem J* **242**, 89–95.

53 Haanstra JR, González-Marcano EB, Gualdrón-López M & Michels PAM (2016) Biogenesis, maintenance and dynamics of glycosomes in trypanosomatid parasites. *Biochim Biophys Acta* **1863**, 1038–1048.

54 Balcazar DE, Vanrell MC, Romano PS, Pereira CA, Goldbaum FA, Bonomi HR & Carrillo C (2017) The superfamily keeps growing: Identification in trypanosomatids of RibJ, the first riboflavin transporter family in protists. *PLOS Negl Trop Dis* **11**, e0005513.

55 Tielens AGM & van Hellemond JJ (2009) Surprising variety in energy metabolism within Trypanosomatidae. *Trends Parasitol* **25**, 482–490.

56 Mantilla BS, Marchese L, Casas-Sánchez A, Dyer NA, Ejeh N, Biran M, Bringaud F, Lehane MJ, Acosta-Serrano A & Silber AM (2017) Proline metabolism is essential for *Trypanosoma brucei* brucei survival in the tsetse vector. *PLoS Pathog* **13**, 1.

57 Matthews KR (2005) The developmental cell biology of *Trypanosoma brucei*. *J Cell Sci* **118** (Pt 2), 283–290.

58 Allmann S & Bringaud F (2017) Glycosomes: a comprehensive view of their metabolic roles in *T. brucei*. *Int J Biochem Cell Biol* **85**, 85–90.

59 Smith TK, Bringaud F, Nolan DP & Figueiredo LM (2017) Metabolic reprogramming during the *Trypanosoma brucei* life cycle. *F1000Res* **6**, 683.

60 Herman M, Pérez-Morga D, Schtickzelle N & Michels PA (2008) Turnover of glycosomes during life-cycle differentiation of *Trypanosoma brucei*. *Autophagy* **4**, 294–308.

61 Bauer S & Morris MT (2017) Glycosome biogenesis in trypanosomes and the de novo dilemma. *PLoS Negl Trop Dis* **11**, e0005333.

62 Engstler M & Boshart M (2004) Cold shock and regulation of surface protein trafficking convey sensitization to inducers of stage differentiation in *Trypanosoma brucei*. *Genes Dev* **18**, 2798–2811.

63 Bachmaier S, Thanner T & Boshart M (2020) Culturing and transfection of pleomorphic *Trypanosoma brucei*. Trypanosomatids: Methods and Protocols. In Methods in Molecular Biology (Michels PAM, Ginger ML & Zilberstein D, eds), pp. 23–38.Springer US, New York, NY.

64 Vassella E & Boshart M (1996) High molecular mass agarose matrix supports growth of bloodstream forms of pleomorphic *Trypanosoma brucei* strains in axenic culture. *Mol Biochem Parasitol* **82**, 91–105.

65 Brun R & Schänenberger M (1979) Cultivation and *in vitro* cloning or procyclic culture forms of *Trypanosoma brucei* in a semi-defined medium. Short communication. *Acta Trop* **36**, 289–292.

66 Bastin P, Bagherzadeh A, Matthews KR & Gull K (1996) A novel epitope tag system to study protein targeting and organelle biogenesis in *Trypanosoma brucei*. *Mol Biochem Parasitol* **77**, 235–239.

67 Wirtz E, Leal S, Ochatt C & Cross GM (1999) A tightly regulated inducible expression system for conditional gene knock-outs and dominant-negative genetics in *Trypanosoma brucei*. *Mol Biochem Parasitol* **99**, 89–101.

68 Burkard G, Fragoso CM & Roditi I (2007) Highly efficient stable transformation of bloodstream forms of *Trypanosoma brucei*. *Mol Biochem Parasitol* **153**, 220–223.

69 Chen X, Zaro JL & Shen W-C (2013) Fusion protein linkers: property, design and functionality. *Adv Drug Deliv Rev* **65**, 1357–1369.

70 Allmann S (2014) Developmental adaptations of energy and lipid metabolism in *Trypanosoma brucei* insect forms. Thesis, Ludwig-Maximilians-Universität München, Germany.
71 Xong HV, Vanhamme L, Chamekh M, Chimfwembe CE, Abbeele JVD, Pays A, Meirvenne NV, Hamers R, Baetselier PD & Pays E (1998) A VSG expression site-associated gene confers resistance to human serum in Trypanosoma rhodesiense. *Cell* **95**, 839–846.
72 Kohl L, Sherwin T & Gull K (1999) Assembly of the paraflagellar rod and the flagellum attachment zone complex during the *Trypanosoma brucei* cell cycle. *J Eukaryot Microbiol* **46**, 105–109.
73 Saas J, Ziegelbauer K, von Haeseler A, Fast B & Boshart M (2000) A Developmentally regulated aconitase related to iron-regulatory protein-1 is localized in the cytoplasm and in the mitochondrion of *Trypanosoma brucei*. *J Biol Chem* **275**, 2745–2755.
74 Bringaud F, Baltz D & Baltz T (1998) Functional and molecular characterization of a glycosomal PPi-dependent enzyme in trypanosomatids: pyruvate, phosphate dikinase. *Proc Natl Acad Sci USA* **95**, 7963–7968.
75 Bringaud F, Peyruchaud S, Baltz D, Giroud C, Simpson L & Baltz T (1995) Molecular characterization of the mitochondrial heat shock protein gene from *Trypanosoma brucei*. *Mol Biochem Parasitol* **74**, 119–123.
76 Bringaud F, Peris M, Zen KH & Simpson L (1995) Characterization of two nuclear encoded protein components of mitochondrial ribonucleoprotein complexes from *Leishmania tarentolae*. *Mol Biochem Parasitol* **71**, 65–79.
77 Deramchia K, Morand P, Biran M, Millerioux Y, Mazet M, Wargnies M, Franconi JM & Bringaud F (2014) Contribution of pyruvate phosphate dikinase in the maintenance of the glycosomal ATP/ADP balance in the *Trypanosoma brucei* Procyclic Form. *J Biol Chem* **289**, 17365–17378.
78 Gärg A, Klaus A, Lück C, Weiland F & Weiss W (2007) Two-dimensional electrophoresis with immobilized pH gradients for proteome analysis. Technische Universität München, Germany.
79 Candiano G, Bruschi M, Musante L, Santucci L, Ghiggeri GM, Carnemolla B, Orecchia P, Zardi L & Righetti PG (2004) Blue silver: a very sensitive colloidal Coomassie G-250 staining for proteome analysis. *Electrophoresis* **25**, 1327–1333.
80 Cox J & Mann M (2008) MaxQuant enables high peptide identification rates, individualized p.p.b.-range mass accuracies and proteome-wide protein quantification. *Nat Biotechnol* **26**, 1367–1372.
81 R Core Team (2019) R: A Language and Environment for Statistical Computing. R Foundation for Statistical Computing, Vienna, Austria.
82 RStudio Team (2016) RStudio: Integrated Development Environment for R. RStudio Inc, Boston, MA.
83 Stothard P (2000) The sequence manipulation suite: javascript programs for analyzing and formatting protein and DNA sequences. *Biotechniques* **28**, 1102–1104.
84 Schindelin J, Arganda-Carreras I, Frise E, Kaynig V, Longair M, Pietzsch T, Preibisch S, Rueden C, Saalfeld S, Schmid B *et al.* (2012) Fiji: an open-source platform for biological-image analysis. *Nat Methods* **9**, 676–682.
85 Mitchell AL, Attwood TK, Babbitt PC, Blum M, Bork P, Bridge A, Brown SD, Chang HY, El-Gebali S, Fraser MI *et al.* (2019) InterPro in 2019: improving coverage, classification and access to protein sequence annotations. *Nucleic Acids Res* **47**, D351–D360.
86 Benson DA, Cavanaugh M, Clark K, Karsch-Mizrachi I, Ostell J, Pruitt KD & Sayers EW (2018) GenBank. *Nucleic Acids Res* **46**, D41–D47.
87 Leys D, Tsapin AS, Nealson KH, Meyer TE, Cusanovich MA & Van Beeumen JJ (1999) Structure and mechanism of the flavocytochrome c fumarate reductase of *Shewanella putrefaciens* MR-1. *Nat Struct Biol* **6**, 1113–1117.